JCTC Journal of Chemical Theory and Computation

Bound Triplet Pairs in the Highest Spin States of Coinage Metal Clusters

David Danovich and Sason Shaik*

The Institute of Chemistry and The Lise-Meitner Minerva Center for Computational Quantum Chemistry, The Hebrew University, Jerusalem 91904, Israel

Received February 14, 2010

Abstract: The work discusses bonding in coinage metal clusters, $^{n+1}M_n$ (M = Cu, Ag, Au), that have maximum spin without a single electron pair. It is shown that the bonding energy per atom, D_e/n, exhibits a strong nonadditive behavior; it grows rapidly with the cluster size and converges to values as large as 16−19 kcal/mol for Au and Cu. A valence bond (VB) analysis shows that this no-pair ferromagnetic bonding arises from *bound triplet electron pairs* that spread over all the close neighbors of a given atom in the clusters. The bound triplet pair owes its stabilization to the resonance energy provided by the mixing of the local ionic configurations, $^3M(\uparrow\uparrow)^- M^+$ and $M^+ {}^3M(\uparrow\uparrow)^-$, and by the various excited covalent configurations (involving p_z and d_{z^2} atomic orbitals) into the fundamental covalent structure $^3(M\uparrow\uparrow M)$ with a s^1s^1 electronic configuration. The VB model shows that a weak interaction in the dimer can become a remarkably strong binding force that holds together monovalent atoms without a single electron pair.

Introduction

No-pair ferromagnetic bonding involves no electron pairing, and the bonding interaction, curiously as it may sound at this point, originates from *triplet electron pairs,* as found, for example, in high-spin alkali metal clusters.[1−6]

To clarify the term no-pair ferromagnetic bonding, consider in Scheme 1a the Li_2 case, where the 2s atomic orbitals form a set of bonding (2σ, i.e., σ_g) and antibonding ($2\sigma^*$ i.e., σ_u) orbitals. In the singlet ground state, the two electrons occupy the bonding orbital to form a Li−Li molecule bound by an electron pair. By contrast, in the triplet $^3\Sigma_u^+$ state, where the electron occupancy is $2\sigma^1 2\sigma^{*1}$, the bond order is formally zero. Indeed, the $2\sigma^1 2\sigma^{*1}$ triplet configuration (Scheme 1a) is equivalent to the purely covalent triplet $2s(1)^1 2s(2)^1$ configuration, in Scheme 1b, where each Li possesses a single electron localized in the respective 2s orbital. This configuration is repulsive and should cause the dissociation of $^3Li_2$. However, the triplet $^3\Sigma_u^+$ state of Li_2 is actually bound,[3] albeit weakly, and the same is true for the other no-pair alkali dimers, which form weakly bonded triplet $^3\Sigma_u^+$ states.[7−10]

As was shown by means of high-level ab initio calculations and valence bond (VB) theory,[3] the weak bonding arises due to the mixing of higher lying ionic and covalent configurations, $2s(1)^1 2p_z(1)^1$, $2s(2)^1 2p_z(2)^1$, and $2p_z(1)^1 2p_z(2)^1$, into the repulsive $2s(1)^1 2s(2)^1$ configuration. Thus, while these additional configurations are high lying, their mixing is still sufficient to overcome the 2s−2s triplet repulsion and to produce a shallow minimum.[3,5,11] As the cluster grows to

Scheme 1. (a) Orbital Mixing of the Pure 2s Atomic Orbitals in $^3Li_2$ and (b) The Equivalence Between $2\sigma^1\ 2\sigma^{*1}$ and $2s(1)^1 2s(2)^1$ Configuration Representations[a]

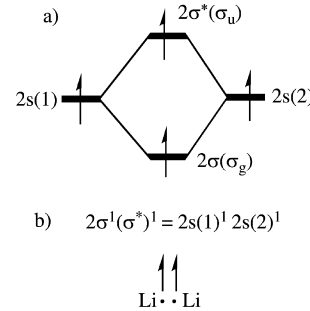

[a] The symmetry labels of 2σ and $2\sigma^*$ are indicated in parentheses. The 1 and 2 in parentheses are atom numbers. The Li···Li moiety lies on the *z*-axis.

* Corresponding author e-mail: sason@yfaat.ch.huji.ac.il.

10.1021/ct100088u © 2010 American Chemical Society
Published on Web 04/14/2010

$^{n+1}Li_n$ with $n > 2$, the number of high-spin ionic and excited covalent configurations increases steeply, so does the binding energy of the cluster, which grows and converges to 12 kcal mol^{-1} per atom, without having a single electron pair.[5] Henceforth, we refer to this type of bonding by the term *no-pair ferromagnetic bonding* (NPFM) bonding. An alternative representation of NPFM bonding was described by McAdon and Goddard,[1] using interstitial orbitals. The two representations are ultimately equivalent.[3,4]

Except for the intellectual interest aroused by this unusual bonding form, some no-pair clusters are real molecular entities, which have actually been made and probed by experimental techniques. Thus, laser-induced emission spectroscopy of the triplet lithium, sodium, potassium, rubidium, and cesium dimers showed a weakly bound $^3\Sigma_u^+$ state.[7−9] In fact, there exists spectroscopic evidence also for the no-pair alkali trimer species ($^4A'$), $^4Li_3$, $^4Na_3$, and $^4K_3$.[12−16] But not only alkali clusters, copper seems also capable of this form of bonding, as may be deduced from the characterization of the $^3\Sigma_u^+$ state of $^3Cu_2$.[17] As such, these no-pair clusters are real entities, which enrich the scope of chemical bonding, and are, therefore, of wide general interest to chemists. An additional interest in this kind of clusters is their relationship to Bose−Einstein condensates in which the quantum states of all atoms are identical and to Fermi-"gases" of fermionic isotopes of alkali metals, (e.g., K with atomic mass 40) in magnetic fields.[16,18] Finally, having maximum magneticity, no-pair clusters are also interesting for their potential applications in nanochemistry.

The present paper constitutes part of our ongoing program[3−6] to map the territory of these no-pair clusters in the periodic table. Coinage metals,[19−21] which possess valence configurations $nd^{10}(n+1)s^1$ that are analogous in a way to the monovalent alkali metals, seem particularly appealing candidates. Thus, in previous studies we compared the NPFM bonding in the clusters of sodium[6] and copper[22] to those of lithium. The sodium clusters $^{n+1}Na_n$ ($n = 2-12$) were found to be much more weakly bound than those of the lithium clusters $^{n+1}Li_n$, whereas the $^{n+1}Cu_n$ ($n = 2-14$) clusters exhibited stronger bonding, reaching 18−19 kcal/mol per atom. Therefore, the no-pair clusters of the coinage metals may be significantly stickier than the corresponding alkali cluster, and especially so the gold cluster where relativistic effects may contribute to this stickiness.[23] In view of the great surge of interest in gold clusters,[24] an investigation of NPFM bonding in $^{n+1}Au_n$ is timely and may be of broad interest. Interestingly, gold surfaces are known to induce sudden magnetization upon adsorption of layers of organic thiols due to formation of "bonded triplet pairs", as proposed by the Naaman et al.[25] The present paper investigates, therefore, NPFM bonding in no-pair coinage clusters of M = Cu, Ag, and Au, and then models the binding energy by a suitable VB model, as done for other no-pair clusters.[3,5,22]

Methods and Details of Calculations

A. Software, Methods, Basis Sets, and Benchmarking. *Software.* All density functional calculations presented here were performed with the Gaussian03 program package.[26] All coupled cluster using single, double, and perturbative triples excitation (CCSD(T)) calculations were carried out with the MOLPRO 2006.1 program package.[27] Ab initio valence bond (VB) calculations were performed with the Xiamen-01 ab initio Valence Bond program[28] using the St-RECP basis set (see below). The VB calculations were used to obtain the repulsive interactions in the purely covalent structure of the dimer with ns^1ns^1 electronic configuration.

Methods and Basis Sets. As has been shown recently,[29] relativistic effects are important for the correct description of properties of the coinage metal clusters and especially for the no-pair states. Therefore, to create a benchmark for the larger clusters, we calculated the ground state and no-pair triplet state of the dimers with the CCSD(T) method using the Douglas−Kroll−Hess (DKH) quasi-relativistic Hamiltonian[30] and the Hamiltonian, which incorporates the relativistic effects via the normalized elimination of small component (NESC) method.[31] Due to program limitation, the truncated (up to f functions) and fully uncontracted aug-cc-pCXZ basis sets of Peterson[32] were used for the NESC method, with X = T, Q, 5.[29] By contrast with the former NESC calculations,[29] in the present DKH calculations, we employed Peterson's standard relativistic aug-cc-pVXZ-DK basis.[32] For comparison, we also tested the non relativistic CCSD(T) method with all-electrons non relativistic Peterson correlation consistent basis sets (aug-cc-PVXZ-NR, where X = T, Q, 5).[32] Since the use of unrestricted coupled cluster (UCCSD(T)) proved to be too time-consuming, even for the dimer, we used density functional theory (DFT) methods for all the higher clusters.

The DKH−CCSD(T) and NESC−CCSD(T) results provided the benchmark for selecting the appropriate density functional/basis set combinations for calculating the larger clusters. To this end, we have examined the applicability of the different density functionals (PW91, B3P86, B3LYP, TPSS, and BMK) with Peterson-type pseudopotential basis sets (aug-cc-pVXZ-PP, where X = T, Q, 5)[33] as well as the B3P86 density functional in combination with the 1997 Stuttgart relativistic small effective core potential (St-RECP) with extended valence basis set (with (8s7p6d)/[6s5p3d] contractions);[34] the latter combination UB3P86/St-RECP was used already in our previous paper on $^{n+1}Cu_n$ clusters.[22] Specifically, UB3P86/St-RECP was shown[22] to have a very small basis set superposition error (BSSE) and was compatible with the results of the extended augmented double-ζ atomic natural orbital (ANO) basis set of Roos et al.[35] As seen below, the best combinations were found to be UB3P86/St-RECP and UB3LYP/aug-cc-pVTZ-PP. For the sake of consistency with our previous studies,[22] the present study uses both methods.

Description of the Benchmark Calculations. The dimers in the ground and no-pair triplet states were used to benchmark the DFT methods against available experimental data, where available, as well as relativistic CCSD(T) calculations with all electrons Peterson basis sets and with aug-cc-pVXZ-PP pseudopotential basis sets of Peterson.[33]

Table 1 shows the equilibrium bond lengths (R_e) and bond dissociation energies (D_e) values for Cu_2 in the ground $^1\Sigma_g^+$ state and in the no-pair $^3\Sigma_u^+$ state with relativistic (RL) and nonrelativistic (NR) CCSD(T) calculations. Inspection of the

Table 1. Results of the Relativistic (RL) and Nonrelativistic (NR) CCSD(T)/aug-cc-pVTZ Calculations of R_e (Å) and D_e (kcal/mol) for the Ground-Singlet and the No-Pair Triplet States of Cu_2

method	R	D_e
	Singlet $^1\Sigma_g^+$	
RL (DKH)	2.224	45.28
NR	2.258	42.51
exptl	2.220[a]	48.208[b]
	Triplet $^3\Sigma_u^+$	
RL (DKH)	2.703	1.328
RL (NESC)	2.711	1.270
NR	2.935	0.735
exptl[c]	2.48	3.46 ± 0.6

[a] From ref 17b. [b] From ref 17c. [c] From ref 17a.

Table 2. R_e (Å) and D_e (kcal/mol) Results for $^3Cu_2$ using Relativistic DKH−CCSD(T) with All-Electron aug-cc-PVXZ Basis Sets and CCSD(T) Calculations with Pseudopotential aug-cc-PVXZ-PP (X = T, Q, 5) Basis Sets

	VTZ[a]	VTZ-PP	VQZ	VQZ-PP	V5Z[a]	V5Z-PP
R_e	2.703	2.689	2.677	2.671	2.662	2.659
D_e	1.328	1.372	1.519	1.614	1.678	1.703

[a] With BSSE correction, R_e = 2.753 Å and D_e = 0.863 kcal/mol for VTZ and 2.670 Å and 1.537 kcal/mol for V5Z.

ground state shows that the difference between relativistic and nonrelativistic calculations is less than 0.04 Å for the equilibrium distance (R_e) and about 3 kcal/mol for the bond dissociation energy (D_e), which is less than 6%. The importance of relativistic effects is much more pronounced for the triplet state of Cu_2. For this state, relativity leads to shortening of R_e by more than 0.2 Å, and it increases the D_e by almost a factor of 2. For the triplet state of the copper dimer, the agreement between two relativistic NESC and DKH methods is quite reasonable (less than 0.01 Å and 0.05 kcal/mol). Furthermore, the match of the relativistic calculations to experimental data is seen to be reasonable.[36]

Table 2 shows the effect of using pseudopotential (PP)-CCSD(T) vs all-electron DKH−CCSD(T) relativistic calculations with matching basis set sizes on the properties of the no-pair state of Cu_2. It is seen that the pseudopotential calculations give reasonable results for the bond length and the bonding energy. The PP calculations always lead to a slightly shorter R_e (0.014 Å for aug-cc-pVTZ-PP and only 0.003 Å for aug-cc-pV5Z basis sets) and a marginally larger D_e value (the discrepancy is less than 0.1 kcal/mol). Therefore, the combination of CCSD(T) with PP basis sets gives good benchmark values that can test DFT methods.

Tables 3 and 4 compares R_e and D_e values in the no-pair triplet states of Cu_2 and Au_2 calculated with CCSD(T)/aug-cc-pVXZ-PP (X = T, Q, 5) and DFT/aug-cc-pVXZ-PP (X = T, Q, 5) methods. Alongside these, we show the less time-consuming B3P86/St-RECP results. All investigated functionals, except for B3LYP/aug-cc-pVXZ-PP (X = T, Q, 5) and B3P86/St-RECP, are seen to considerably overestimate the bond dissociation energies (D_e) in comparison with the benchmark CCSD(T) values and with the experimental datum[17a] of 3.46 ± 0.6 kcal/mol. It should be noted that the experimentally measured values for the triplet electronic state reported in Table 1 were obtained from laser spectroscopic

Table 3. R_e (Å) and D_e (kcal/mol) Results for $^3Cu_2$ using CCSD(T) and Different Density Functionals with Pseudopotential Basis Sets aug-cc-pVXZ-PP (X = T, Q, 5) and B3P86/St-RECP

	PW91	B3P86	B3P86	B3LYP	TPSS	BMK	CCSD(T)
			R_e				
pVTZ-PP	2.464		2.532	2.590	2.452	2.606	2.689
pVQZ-PP	2.464		2.532	2.590	2.451		2.671
pV5Z-PP	2.462		2.530	2.586		2.617	2.659
St-RECP		2.607					
			D_e				
pVTZ-PP	12.28		4.295	2.440	11.396	8.036	1.372
pVQZ-PP	12.28		4.284	2.414	11.395		1.614
pV5Z-PP	12.36		4.301	2.452		10.82	1.703
St-RECP		3.047					

Table 4. R_e (Å) and D_e (kcal/mol) Results for $^3Au_2$ using CCSD(T) and Different Density Functionals Methods with Pseudopotential aug-cc-pVXZ-PP (X = T, Q, 5) Basis Sets and B3P86/St-RECP

	B3P86	B3P86	B3LYP	TPSS	BMK	CCSD(T)
		R_e				
pVTZ-PP	2.795		2.875	2.7423	2.920	2.890
pVQZ-PP	2.793		2.872	2.7395	2.917	2.872
pV5Z-PP	2.790		2.869			2.866
St-RECP		2.932				
		D_e				
pVTZ-PP	6.403		3.988	10.724	4.683	3.767
pVQZ-PP	6.421		4.035	10.852	4.812	4.214
pV5Z-PP	6.454		4.094			4.301
St-RECP		4.415				

measurements on a matrix isolated copper dimer.[17a] The uncertainty in such a measurement makes it difficult to estimate, e.g., the matrix effects upon the electronic transitions of Cu_2, which could be significant. For this reason, this experimental D_e value may contain significant uncertainty.[17a] Since the bond dissociation energy is the key factor in our study, we rely henceforth on the UB3LYP/aug-cc-pVTZ-PP and UB3P86/St-RECP for calculating the larger clusters.

B. Geometry Optimization, State Identification, and Bond Dissociation Energy Calculations. *Geometry Optimization.* Different structures with different state symmetries were tested for each cluster size in order to find the most stable clusters. All calculations discussed here are the result of a full geometry optimization followed by the usual test for genuine minima using frequency calculations.

Tests for State Identity. For every cluster we used the TDDFT method, as a stability check, to ascertain the lowest energy solution for the ground and the no-pair states. The TDDFT tests were carried out with NWCHEM 5.1[37] and Gaussian03 programs. In the event where the tested state did not have the lowest solution in the TDDFT calculation, a new guess function was examined, and the geometry was reoptimized until the TDDFT calculation converged to the lowest one.

Since there is no guarantee that the no-pair states will be the lowest state of a given multiplicity for a particular cluster, we routinely verified that the singly occupied orbitals in the state of choice were *only* the σ-types. These orbitals were examined in two ways: (i) Initially, using canonical

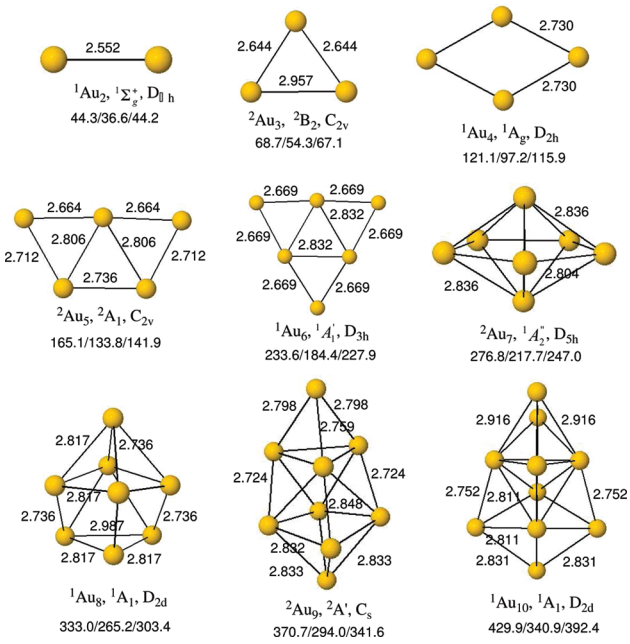

Figure 1. UB3P86/St-RECP optimized structures with their point groups and state assignments for the most stable coinage metal clusters in their ground electronic states. The bond length values are shown only for Au_n. Bond dissociation energies (D_e, in kcal/mol) are shown below the structures in the order Cu/Ag/Au.

Kohn−Sham (KS) orbitals, we made sure that no radial orbitals (perpendicular to the surface of the cluster and, hence, not of a σ M−M character) were singly occupied. (ii) Subsequently, these singly occupied KS orbitals were localized, and the resulting orbitals were ascertained to be largely (98%) confined to a single atom and to be dominated by the highest s-type AO of Cu, Ag, or Au atoms.

Bond Dissociation Energy Calculations. The dissociation energies and the dissociation energies per atom, D_e and D_e/n, were corrected for BSSE. BSSE on the D_e and D_e/n values were found using the counterpoise method (using the keyword counterpoise = n [n is a number of coinage atoms in the cluster] in Gaussian-03). In our previous study,[22] it was found that BSSE values are very small and do not change the behavior of D_e/n vs the cluster size n. Thus, the BSSE corrected and uncorrected of D_e/n vs n plots are virtually parallel to one another, different by almost a constant quantity (see Supporting Information, Figure S1). For this reason, in the present analyses, we used BSSE uncorrected values of D_e/n for all coinage metals. The study generated many results that are summarized in the Supporting Information.

Results

A. Ground State Structures of Coinage Metal Clusters. The geometry optimization in the ground and no-pair states revealed several "geometric isomers" for each studied cluster size. Figure 1 displays the UB3P86/St-RECP optimized structures of the most stable geometric isomers of the coinage metal clusters, M_n, where n varies from 2 to 10. The point group symmetries are common to all the M_n clusters for a given n. Therefore, to compact the information,

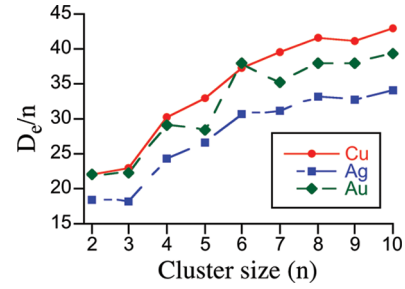

Figure 2. Dependence of the bond dissociation energies per atom (D_e/n, in kcal/mol) on the cluster size for the ground states of the coinage metal clusters, M_n. Copper data is in red, silver is in blue, and gold is in green.

we show in Figure 1 bond lengths only for the Au_n clusters, while the rest of the bond lengths and other geometric parameters are given in the Supporting Information, Tables S1−S3 and Figures S2 and S3.

It is seen from Figure 1 that for $n = 2-6$, the most stable isomers of the ground-state M_n clusters are two-dimensional (2D) structures. Starting with $n = 7$ and on to larger clusters, the most stable structures are seen to be three-dimensional.[38] These point-group symmetries and geometries are virtually the same as those published recently for the ground states of Ag_n,[39] using the spin-unrestricted Perdew and Wang (PW91) density functional method implemented in the Demon-KS3P5 program package with the all-electron orbital basis set contracted as (633321/53211*/521+) and in conjunction with the corresponding (5,5;5,5) auxiliary basis set for describing the s, p, and d orbitals. This match of the results for different functionals implies that the most stable structures obtained in our calculations are most likely independent of the density functionals and basis sets.

The numbers underneath the structures in Figure 1 correspond to the total D_e, in kcal/mol, in the order Cu/Ag/Au. It is seen that the ground state of the coinage metal clusters, even for the dimer, has significant bonding energies. The D_e increases considerably by about 10 times, reaching values of 340−430 kcal/mol for $n = 10$.

If, however, we consider the bond dissociation energy per atom (D_e/n), which is one of the measures of cluster stability, we find that the D_e/n quantity does not change as drastically as the total D_e. As can be seen in Figure 2, the D_e/n increases by less than a factor of 2 from the dimer to the M_{10} cluster and reaches the value around 40 kcal/mol. As shall be seen later, this is very different from the behavior we found for the no-pair states of the coinage metal clusters.

One of the important geometric features of the cluster is an average bond length between the first-neighbor bonded atoms. Since all the M_n clusters show similar trends, we have shown in Figure 3 the variation of this distance only for Au_n clusters. It is seen that the average bond length of the ground-state clusters falls into three distinct areas: the dimer, which has the shortest bond length, the planar clusters with $n = 3-6$, possessing intermediate bond lengths, and the three-dimensional (3D) clusters with $n > 6$, which exhibit the longest bond lengths. Thus, the average distance depends on the dimensionality of the clusters, and the changes within each group are smaller than between the groups. Comparison

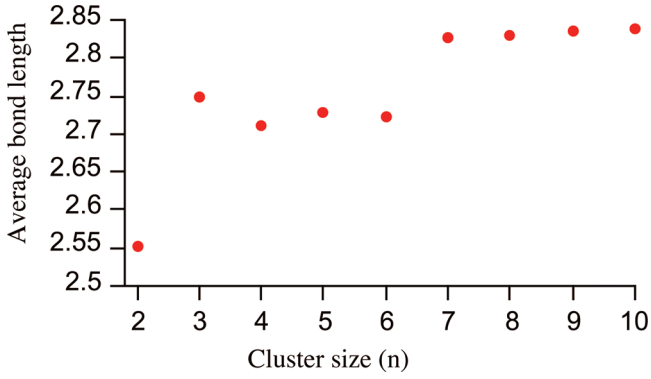

Figure 3. Dependence of the average first-neighbor bond lengths (in Å) of ground state of gold clusters plotted against the cluster size.

of Figures 2 and 3 shows that D_e/n increases as the average bond lengths between the first-neighbor-bonded atoms increases. The reason for this seemingly counterintuitive behavior is because as one moves from the dimer to the large clusters, the number of the bonds per atom increases; thus, the average number of the bonds per atom is 0.5 for the dimer, 1−1.5 for the 2D clusters, and 2−2.4 for the 3D-clusters, which belong to the 3D group. As such, while each particular bond in the large clusters becomes weaker, as in the smaller ones, the total bond dissociation energy increases considerably due to the much larger number of the bonds. Later this behavior too will be contrasted with the trend exhibited by the no-pair state of the coinage metal clusters.

B. Structures of Coinage Metal Clusters in the No-Pair State. In contrast to the ground state, where 3D sets in only for clusters with $n \geq 7$, the most stable no-pair state structures have 3D geometries starting already with $^5M_4$, which is tetrahedral.[40] These clusters are depicted in Figure 4, which displays the UB3P86/St-RECP geometries; the UB3LYP/aug-cc-pVTZ-PP geometries follow the same trends and are relegated to the Supporting Information (Figures S6 and S7 and Tables S7 and S8). The bond lengths are indicated in Figure 4 only for $^{n+1}Au_n$, and the data for the other metals are given in the Supporting Information (Tables S4−S6 and Figures S4 and S5).

As we found for the ground state, the most stable geometries of the no-pair clusters in Figure 4 are very similar for all coinage atoms. Only two exceptions exist for the clusters with $n = 5$ and 6, where the most stable isomer depends on the metal, as seen in Figure 5. Thus, in the case of $^6M_5$, one finds trigonal-bipyramidal or square-pyramidal structures depending on M, but the difference in the total energy of the two isomers for a given metal is small, e.g., for $^6Au_5$ the total energy difference is only 2.8 kcal/mol. The same applies to $^7M_6$: the total energy difference between the alternative structures for a given metal is small. The unusual C_{2v} structure of $^7Cu_6$ cluster was created by adding the sixth copper atom to one of the faces of the trigonal-bipyramidal structure, while keeping other bonds, as in the D_{3h} structure of $^6Cu_5$ cluster.

At present, we do not have an explanation for these structural variations for $n = 5$ and 6, and perhaps such an explanation is not warranted, since the relative energies of the isomers are very close. For all other clusters, the

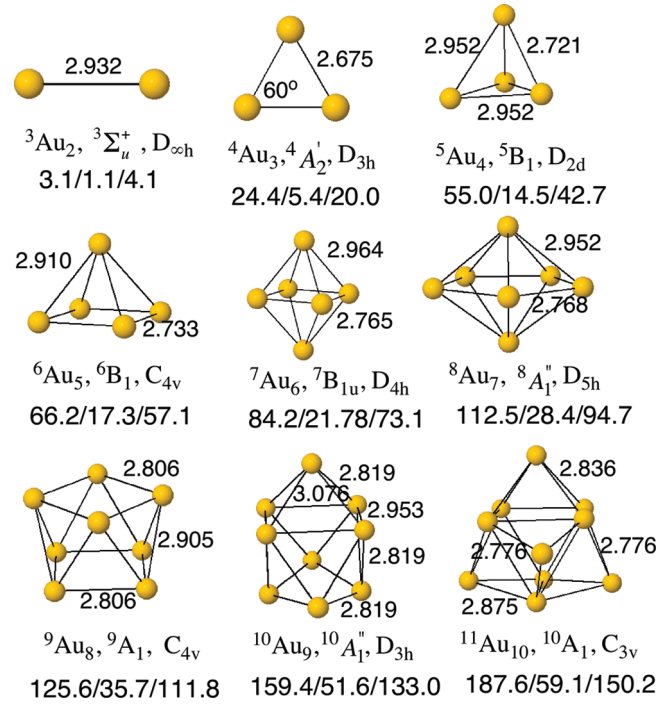

Figure 4. UB3P86/St-RECP optimized structures, their point groups, and state assignments for the most stable coinage metal clusters in the no-pair high-spin states, $^{n+1}M_n$. The bond length values are shown only for $^{n+1}Au_n$. Bond dissociation energies (D_e, in kcal/mol) are shown below the structures in the order Cu/Ag/Au.

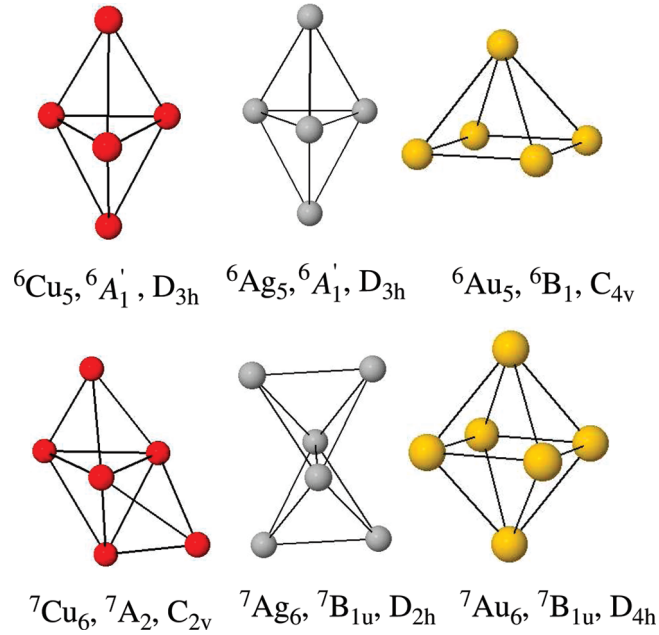

Figure 5. UB3P86/St-RECP optimized structures for $^6M_5$ and $^6M_5$ clusters, their point groups, and state assignments.

structures are metal-independent and are close to being highly symmetrical species. For example, the D_{2d} symmetry of the $^5M_4$ clusters (Figure 4) is actually very close to a pure tetrahedral T_d symmetry. Indeed, except for the clusters with $^8M_7$, generally the point-group symmetry of the no-pair clusters is always higher than the symmetry of the corresponding clusters in their ground state. Moreover, in previous alkali metal clusters, we noted the same phenomenon,[3,22]

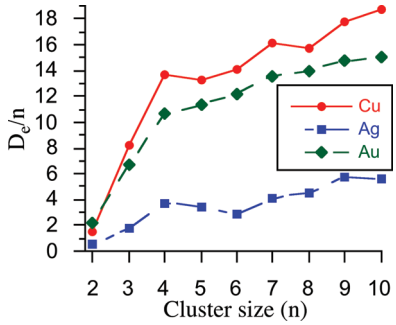

Figure 6. Dependence of the bond dissociation energies per atom, D_e/n (in kcal/mol), on cluster size for the no-pair states of the coinage metal clusters.

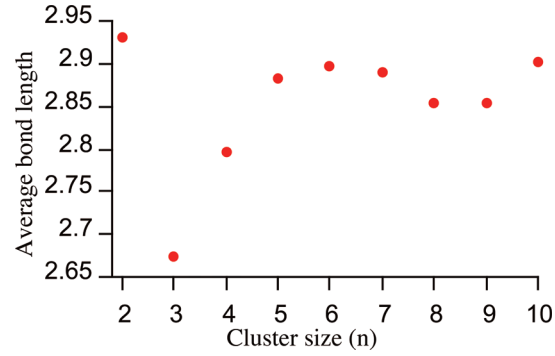

Figure 7. Dependence of the average bond length between the first-neighbor-bonded atoms (in Å) for gold clusters in the high-spin state plotted against the cluster size.

Table 5. D_e/n Values (in kcal/mol) Calculated for No-Pair States, $^{n+1}M_n$, of the Copper and Gold Clusters Using UB3LYP/aug-cc-pVTZ-PP and UB3P86/St-RECP Methods

	UB3LYP/ aug-cc-pVTZ	UB3P86/ St-RECP		UB3LYP/ aug-cc-pVTZ	UB3P86/ St-RECP
Cu_2	1.22	1.52	Au_2	1.99	2.21
Cu_3	9.07	8.14	Au_3	9.33	6.67
Cu_4	12.94	13.73	Au_4	11.58	10.68
Cu_5	11.39	13.23	Au_5	11.73	11.41
Cu_6	12.29	14.03	Au_6	11.42	12.18
Cu_7	13.80	16.07	Au_7	12.54	13.52
Cu_8	13.49	15.59	Au_8	12.90	13.98
Cu_9	14.85	17.71	Au_9	13.25	14.78
Cu_{10}	15.68	18.76	Au_{10}	13.46	15.02

and hence we are seeing a topological behavior of NPFM bonding, which seems to transcend the identity of the metal. In fact, as we argued before,[3,22] this behavior of the no-pair state is predictable based on VB theory, which shows that the high-spin state clusters attempt to create structures that maximize the coordination number for each atom in the cluster and minimize the repulsive interaction in the fundamental all-s[1] configuration. Generally, the minimized repulsive interaction requires identical bond lengths, and a maximal coordination number means also that the structure has the most symmetrical 3D packing.

It is also interesting to point out the difference between some structures calculated previously with the UB3P86/LANL2DZ method[22] and those obtained in present paper at the B3P86/St-RECP level. There are two main differences. First, the $^6Cu_5$ cluster was previously assigned a C_{4v} point-group symmetry, and now it has D_{3h} symmetry for the most stable structure. At the B3P86/St-RECP level, the difference in the total energy between two structures is 3.3 kcal/mol in favor of D_{3h} symmetry. Second, the $^9Cu_8$ cluster, had a C_{2v} symmetric structure in our previous work,[22] and here it has C_{4v} symmetry, but the difference in total energies between C_{2v} and C_{4v} point group symmetries is negligible. Clearly, the no-pair clusters may exhibit also some fluxionality in their structures.

The total D_e values noted in Figure 4, underneath the structures, exhibit a behavior very different than the trend in ground-state clusters. Thus, D_e starts from a very small value for dimers and increases steeply for the larger no-pair clusters, reaching values that are 50-fold larger than the D_e for the dimers. For example, the D_e for the no-pair dimers of copper and gold is only 3−4 kcal/mol, and it reaches values around 170 kcal/mol for the $^{11}M_{10}$ (M = Au, Cu). As will be discussed, this nonadditive behavior can also be predicted using our VB model of bonding.[3,22]

Let us consider now the D_e/n quantity, which is a measure of the cluster stability. As can be seen from Figure 6, D_e/n increases dramatically by about 10−15 times in contrast with the ground state, where it increased by less than a factor of 2. Thus, the value starts from less than 1 kcal/mol for the dimers and reaches 18 and 15 kcal/mol for copper and gold atoms, respectively, which are remarkably high binding energies for clusters with no electron pairing. The no-pair silver clusters are rather weakly bonded, and the D_e/n value converges to less than 6 kcal/mol at $^{11}Ag_{10}$. In all the series, the steepest increase of D_e/n occurs in the transition from the dimer to the trimer. Another significant increase of D_e/n occurs also between the trimer and the tetramer. According to our VB model, which will be discussed later, this behavior is associated with the very significant increase in the total coordination number of the cluster; from 2 for $^3M_2$ to 6 for $^4M_3$ and then to 12 for $^5M_4$. Further changes in the total coordination number become less considerable for the larger clusters (18 for $^6M_5$, 24 for $^7M_6$, and 30 for $^8M_7$).

The dependence of the average bond length between first-neighbor-bonded atoms on the size of the cluster in the no-pair states of the gold is presented in the Figure 7. The trend is again similar for all other coinage metals, and for this reason, we present here only the results for the gold clusters. As we pointed out above, this dependence in the no-pair state is very different from the trend we found for the ground state. The longest bond distance is observed in the dimer, and it decreases significantly, by about 0.3 Å, for the trimer, which has the shortest bond length among all cluster sizes. For the tetramer, the average bond length increases by about 0.15 Å, and starting from $n = 5$, the average Au−Au distance changes very little in the range of 2.85−2.90 Å.

Discussion

Bonding in the ground-state clusters is relatively easy to understand since it derives from electron pairing and from delocalization of the electrons.[22,41] The intriguing finding is the significant bonding in the states where all the spins are up. To aid the discussion, we display in Table 5 the computed bond dissociation energy per atom (D_e/n) for the no-pair

Table 6. B3P86/St-RECP Calculated and VB Model Estimated BDE/n (kcal/mol) for the No-Pair States of Coinage Metal Clusters

	BDE/*n*					
	Cu		Ag		Au	
n	DFT	model[a]	DFT	model[b]	DFT	model[c]
2	1.52	1.72	0.54	0.84/0.15	2.21	2.16
3	8.14	8.75	1.80	2.34/2.67	6.67	7.09
4	13.73	12.12	3.63	3.38/3.56	10.68	10.11
5	13.23	14.15	3.45	4.01/4.09	11.41	11.65
6	14.03	15.51	3.64	4.07/4.10	12.18	13.14
7	16.07	16.47	4.05	4.73/4.70	13.52	14.01
8	15.70	15.34	4.46	4.41/4.37	13.98	13.05
9	17.71	16.93	5.73	4.88/4.81	14.78	14.45
10	18.76	18.21	5.91	5.26/5.16	15.02	15.56
11		18.58		5.38/5.25		15.89
12		19.50		5.65/5.51		16.70
13		19.43		5.63/5.48		16.65
14		19.37		5.62/5.46		16.59

[a] $\delta\varepsilon_{rep}$ = 16.42 and $\delta\varepsilon_{mix}$ = 1.3245 kcal/mol for Cu. [b] The values for Ag correspond to the two alternative fits: the two-parameter fit ($\delta\varepsilon_{rep}$ = 0.8029 and $\delta\varepsilon_{mix}$ = 0.1653 kcal/mol) and the one-parameter fit ($\delta\varepsilon_{rep}$(VB) = 8.602 and $\delta\varepsilon_{mix}$ = 0.5931 kcal/mol). [c] $\delta\varepsilon_{rep}$ = 6.0256 and $\delta\varepsilon_{mix}$ = 0.6902 kcal/mol for Au.

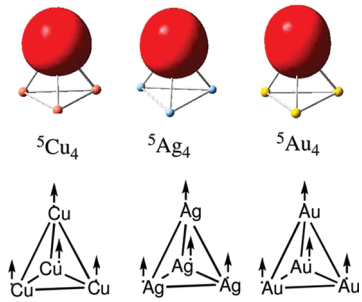

Figure 8. Localized orbitals for $^5M_4$; M = Cu, Ag, Cu. For each cluster, we show only one orbital. Below these orbitals are schematic representations of the electronic structures of these clusters, using dots to represent the electrons and arrows to represent the spin.

states of copper and gold clusters at the UB3LYP/aug-cc-pVTZ-PP and UB3P86/St-RECP levels of theory. The values for silver were obtained only at the UB3P86/St-RECP level and are shown in Table 6.

Inspection of Table 5 shows that, except for the $^4Au_3$ case, the agreement between both methods is quite reasonable, with UB3P86/St-RECP giving a generally larger D_e/n. The converged D_e/n values at $^{11}M_{10}$, for M = Cu and Au, are very impressively large, and they are certainly not weak van der Waals interactions; they are more in the realm of chemical bonds. These values become all the more impressive when one looks at the localized orbitals of the no-pair clusters. Figure 8 shows one of these orbitals for the $^5M_4$ clusters (M = Cu, Ag, Au) which, according to the natural localized molecular orbital (NLMO) analyses,[41] are 98.2% localized with small tails on other atoms. Thus, it is apparent that the electronic structure is largely localized with one electron per site, all the electrons having parallel spins, and that the local orbitals have dominant *n*s (*n* = 4−6 for M = Cu, Ag, Au) characters with some outward hybridization.

So where does the NPFM bonding come from? Why does it get so strong as the cluster increases and then converges very quickly at about *n* = 10? Can we account for the jumps in the D_e/n quantity? What happens as we change M from Cu to Ag and then to Au? Is it possible to find a rationale for the symmetric clusters and for the high coordination numbers that typify these clusters? This will be done by using VB theory and by modeling of the D_e/n quantity.

Scheme 2. (a) Some of the VB Configurations That Contribute to NPFM Bonding in the No-Pair Dimers[a] and (b) The Corresponding VB-mixing diagram[b]

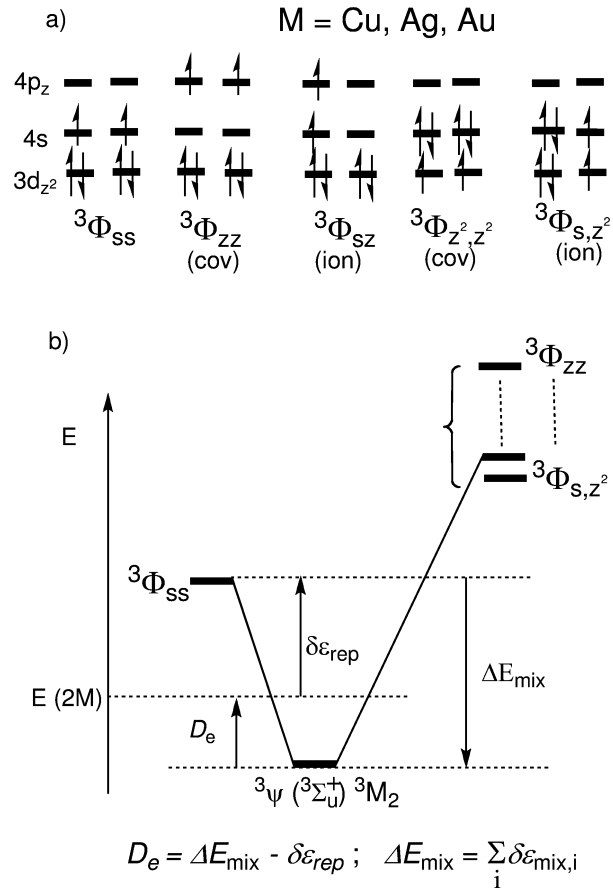

[a] $^3M_2(^3\Sigma_u^+)$ for M = Cu, Ag, and Au. [b] The equation in part (b) is the bond dissociation energy (D_e) expression.

A. Valence Bond Analyses of the NPFM Bonding in the No-Pair States of the Coinage Metal Clusters. As was argued previously,[3,6,22] NPFM bonding originates due to the *ionic-covalent fluctuations of the triplet pairs*. The various types of VB structures that contribute to the wave function of the $^3M_2$ coinage metal dimers as well as the corresponding VB mixing diagram that leads to NPFM bonding are shown in Scheme 2.

Thus, as shown in Scheme 2a, the fundamental configuration is the covalent $^3\Phi_{s,s}$ with the two valence electrons in the (*n*+1)s AOs (4s, 5s, 6s) of the two coinage metal atoms. There are higher-lying VB structures, which involve singly occupied *n*d$_{z^2}$ (*n* = 3−5) and (*n*+1)p$_z$ AOs. Some of these are ionic triplet configurations, like $^3\Phi_{s,z^2}$, which involves electron transfer from the *n*d$_{z^2}$ AO of one metal to the (*n*+1)s AO of the second or from $^3\Phi_{s,z}$, which involves an electron transfer from the (*n*+1)s AO of one atom to the (*n*+1)p$_z$ AO of the second. In addition, there are excited covalent

configurations, where the two valence electrons occupy the $(n+1)p_z$ AOs of the two atoms, as in $^3\Phi_{z,z}$, or the nd_{z^2} AOs of the two atoms, as in $^3\Phi_{z^2,z^2}$. By itself, the fundamental $^3\Phi_{s,s}$ configuration is purely repulsive, and the repulsive term $\delta\varepsilon_{rep}$, in Scheme 2b, arises from the two triplet electrons as well as from the $d^{10}-d^{10}$ closed shell Pauli repulsions. The NPFM bonding will arise only from the mixing of the excited ionic and covalent configurations, each of which contributes a $\delta\varepsilon_{mix,i}$ element as shown in Scheme 2b. Thus, at a given M−M distance, the net NPFM bonding will be a balance between the repulsive interactions in the fundamental structure ($\delta\varepsilon_{rep}$) and the sum of the mixing interaction terms due to all the excited configurations ($\Delta E_{mix} = \sum_i \delta\varepsilon_{mix,i}$). As we move to larger and larger clusters, there will always be one fundamental configuration with a singly occupied *n*s orbital for each atom, $^{n+1}\Phi_{s1,s2,\ ...,\ sn}$. However, now the number of excited ionic and covalent configurations increases in a nonlinear manner, since each atom can have ionic and covalent triplet configurations with each neighboring atom, thus dramatically augmenting the stabilization energy.

As we showed previously,[3,6] the bond dissociation energy (D_e) due to NPFM bonding can be expressed in a simple analytical form. Thus, assuming that the elementary repulsion term ($\delta\varepsilon_{rep}$) is the same for all pairs of bonded atoms and that it involves only the close neighbor atoms, this allows us to use the repulsion term extracted from a VB calculation of the respective dimer molecule and to evaluate the total repulsion by multiplying this pair repulsion by the number of close neighbor M···M pairs in the cluster. In addition, assuming for simplicity that the various excited configurations contribute each an identical close-neighbor mixing term $\delta\varepsilon_{mix,i}$, which is the same as in the corresponding dimer $^3M_2$, allows us to evaluate the total mixing term for any cluster size. This is done by simply counting the number of ionic and covalent excited configurations a given atom has with its close neighbors and by multiplying the resulting number of configurations by the elementary mixing term. We further truncate the number of excited configurations to the lowest excitations involving electron shifts from the *n*d AOs to singly occupied $(n+1)$s AOs and from $(n+1)$s to $(n+1)$p.

These simplifications allow us to model the NPFM-binding energy based on eq 1:

$$D_e = \left[\frac{(N_{AO}^2 + 9)C_{tot}}{2} + N_{AO}\right]\delta\varepsilon_{mix} - \frac{C_{tot}\delta\varepsilon_{rep}}{2} \quad (1)$$

Here N_{AO} is the number of singly occupied and virtual AOs (per atom) that participate in the populating of the *n*-electrons in $^{n+1}M_n$, while C_{tot} is the total coordination number that sums all the close neighbors of all atoms in the cluster. Only s- and p-AO's are counted for N_{AO}. Details of the deriving equaition 1 can be found in the Supporting Information, VB Model equations section.[22]

Due to limitations of the VB software,[28] we are able to calculate only the energy of the fundamental configuration, $^3\Phi_{s,s}$, and evaluate thereby the pair repulsion term in the $^3M_2$ species. The mixing terms are then obtained by least-squares fitting of eq 1 to the computed D_e/n quantities. To test the fit quality, we used a second method whereby we fit eq 1 by least-squares fitting of both the repulsion and the mixing terms. We have checked both approaches and obtained results that are quite similar and are all given in the Supporting Information (Figures S8−S11).

Using UB3P86/St-RECP D_e/n data, the best-fitted pair-repulsion terms are 16.42 for Cu, 6.0256 for Au, and 0.8029 kcal/mol for Ag atoms. The values for $^{n+1}Cu_n$ and $^{n+1}Au_n$ are much larger than those obtained for $^{n+1}Li_n$, which makes physical sense since the coinage metals have in addition $d^{10}-d^{10}$ repulsive terms, which the Li cluster does not have. Indeed, the VB calculated repulsion terms are 14.28 for Cu (at $R_e = 2.60$ Å) and 11.76 kcal/mol for Au (at $R_e = 2.93$ Å), which, while not identical to the fitted values, are large, in the right order, and much larger than the corresponding elementary repulsion calculated by VB for Li (1.504 kcal/mol[3]). The smaller repulsion of Au vs Cu may well reflect the relativistic shrinkage of the 6s orbitals of Au, which lower the $6s^1-6s^1$ repulsion. The fitted $5s^1-5s^1$ repulsive term of Ag is much too small, and this may reflect the poorer quality of the fit. Indeed, the VB calculation for the $5s^1-5s^1$ fundamental structure of $^3Ag_2$ gives significant values, which depends on the equilibrium distance taken for the dimer; 8.602 (at $R_e = 3.12$ Å) and 5.902 kcal/mol (at $R_e = 3.35$ Å, which is obtained with CCSD(T)/St-RECP calculations).

The best-fitted elementary mixing terms are 1.3245, 0.6902, and 0.1653 kcal/mol for Cu, Au, and Ag atoms. The relative ordering of these values is in line with the calculated d−s orbital energy gaps for the atoms (see Supporting Information, Tables S9 and S10). According to the VB mixing model (Scheme 2), larger gaps will result in small mixing terms and vice versa for smaller gaps. The gaps can in turn be understood based on various effects that have been discussed by Pyykkö and Desclaux.[42] Thus, Cu is affected by the "$3d^{10}$ contraction" and hence the 3d−4s gap should be smaller than the 4d−5s gap in Ag, while in Au, the 5d−6s gap shrinks relative to Ag by the relativistic shrinkage.[42] Further support of these considerations is provided by inspecting the σ and σ^* orbitals of the M_2 dimers, which shows that Cu has the largest d contribution, while Ag has the smallest. All the dimers have as well $(n+1)$p contributions to the σ and σ^* orbitals, but these contributions are quite similar to the three atoms. Thus, the order of the mixing terms ($\delta\varepsilon_{mix}$), obtained from the two-parameter fit, is physically reasonable. Again, the $\delta\varepsilon_{mix}$ obtained for Ag from the two-parameter fit procedure may seem very small. Using the VB computed $\delta\varepsilon_{rep}$ gave values of $\delta\varepsilon_{mix} = 0.5931$ kcal/mol, which is still smaller than the corresponding values for Cu and Au.

Inserting these fitted values into the eq 1 enables us to calculate D_e/n values for the larger clusters. All the D_e/n values are collected in Table 6, along with the UB3P86 computed ones. Figure 9 shows plots of the VB modeled and UB3P86 computed D_e/n values for the $^{n+1}Cu_n$, $^{n+1}Au_n$, and $^{n+1}Ag_n$ clusters vs the cluster size *n*.

It is apparent from Table 6 that the quality of the fit is very good for Cu and Au, having R^2 values of 0.97 and 0.98 for Cu and Au, respectively, and of a lesser quality for Ag atoms with $R^2 = 0.89$. However, taking the series together, it is clear that the VB model describes well the entire pattern

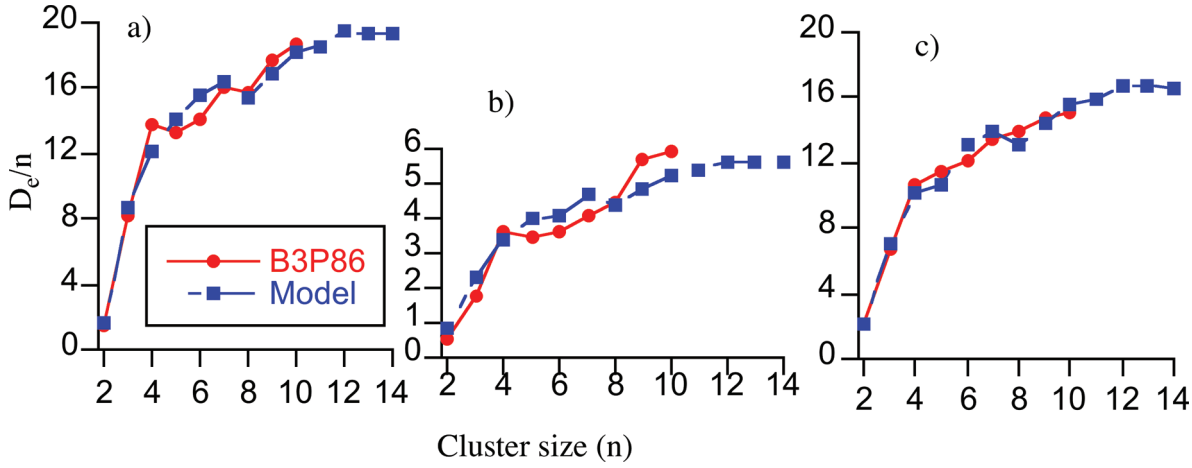

Figure 9. Fit between UB3P86/RECP calculated (red) for (a) copper, (b) silver, and (c) gold clusters and VB model estimated D_e/n (blue) (in kcal/mol) as function of cluster size.

of NPFM bonding in these three coinage metals. Furthermore, as shown in the Supporting Information (Figures S8−S11), the quality of the fits is retained with different combinations of the parameters. Furthermore, inspection of Figure 9 shows that the VB-modeled D_e/n curve fits nicely the UB3P86 calculated one. The VB-modeled curve reproduces the steep rise of the D_e/n observed when moving from $^3M_2$ to $^{n+1}M_n$ clusters, and it converges at approximately 19.5, 16.5, and 5 kcal/mol for the copper (Figure 9a), the gold (Figure 9c), and the silver (Figure 9b), respectively.

The VB model can be used also to account for the seemingly odd behavior of the Cu vs Au clusters. Thus, as can be seen in the Tables 5 and 6, $^3Au_2$ is more strongly bound than $^3Cu_2$. By contrast, as the cluster grows, the trend is reversed, and for the $^{n+1}M_n$ clusters with $n > 10$, the Cu clusters are more strongly bonded with a converged D_e/n value of 19.4 kcal/mol relative to 16.6 kcal/mol for the Au clusters. The VB model in Scheme 2b and eq 1 nicely explains this reversal. Thus, eq 1 shows that the total D_e is a balance between the mixing and repulsion terms with a larger multiplier for the $\delta\varepsilon_{mix}$ term (in eq 1) compared with that of the $\delta\varepsilon_{rep}$ term. This larger multiplier signifies the fact that the number of excited VB configurations, which can mix into the fundamental VB structure, increases much faster than the number of pair repulsions as the cluster grows. Thus, the dimer $^3Cu_2$, with the larger repulsive term, is more weakly bound compared with $^3Au_2$. However, as the cluster grows, the number of contributing VB configurations increases and the total mixing term starts to dominate, and, since the elementary mixing term for Cu is significantly larger than the corresponding one for Au, the D_e and D_e/n values for the $^{n+1}Cu_n$ clusters become larger than for those of the $^{n+1}Au_n$ clusters.

B. NPFM Bonding of Resonating Bound Triplet Pairs. The above discussion shows that the VB modeling inherent in eq 1 captures qualitatively and semiquantitatively the essence of the NPFM bonding in the no-pair clusters of the coinage metals. NPFM bonding arises primarily from bound triplet electron pairs that spread over all the close neighbors of a given atom in the clusters.

The bound triplet pair owes its stabilization to the resonance energy provided by the mixing of the local ionic configurations, $^3M(\uparrow\uparrow)^-M^+$ and $M^+\,{}^3M(\uparrow\uparrow)^-$, and the various excited covalent configurations (involving p_z and d_{z^2} AOs) into the fundamental covalent structure $^3(M\uparrow\uparrow M)$ with the s^1s^1 electronic configuration. As was demonstrated for $^{n+1}Li_n$ clusters,[5] the mixing of the excited covalent structures into $^3(M\uparrow\uparrow M)$ generates a covalent structure with hybrid orbitals that keep the triplet electrons further apart compared with the fundamental s^1s^1 structure and thereby lowers the triplet repulsion. This is augmented by the mixing of the ionic structures, which buttress the bonding by covalent−ionic resonance energy.[43] Thus, if we consider each diatomic triplet pair and its ionic plus covalent fluctuations as a local NPFM bond, we can regard the electronic structure of a given $^{n+1}M_n$ cluster as *a resonance hybrid of all the local NPFM bonds that each atom forms with all of it close neighbors*.

In the case of alkali metals, the local FM bond involves only two electrons in s and p orbitals, while in the coinage metal clusters, there are also filled 3d orbitals that contribute components of three electron bonding due to the participation of these orbitals in the ionic fluctuations (Scheme 2). Thus, the no-pair coinage metal clusters are more strongly bonded than the corresponding alkali metal clusters.[4−6] Moreover, both $^{n+1}Cu_n$ and $^{n+1}Au_n$ possess stronger binding energies than the corresponding $^{n+1}Li_n$ clusters.

Concluding Remarks: Bonded Triplet Pairs

The paper discusses no-pair ferromagnetic (NPFM) bonding in the maximum-spin states of coinage metal clusters as a result of *bonded triplet pairs.* It is shown that the bonding energy per atom, D_e/n, grows rapidly with the cluster size, exhibits a strongly nonadditive behavior, and converges to values as large as 16−19 kcal/mol for gold and copper; values which are of the order of normal spin-paired bonds in metals.

The valence bond analysis of the problem shows that a weak stabilization of the triplet pair in the dimer can become a remarkably strong force that binds together monovalent atoms without a single electron pair. This is achieved because the steeply growing number of VB structures exerts on the triplet pair a cumulative effect of stabilization that is maximized when the cluster is compact with an optimal

coordination number of the atoms. Thus, *the nonadditive behavior of the binding energy is scaled by the number of VB structures available for mixing with the fundamental repulsive structure*, $^{n+1}\Phi_{s(1),\ ...,\ s(i),\ ...,\ s(n)}$.

A more complete mini-periodic table of NPFM bonding will have to include the heavy alkali metals (K, Cs, Fr) and the group III metalloids, like B, Al, and so on. In view of the importance of the ionic structures, the heteroatomic clusters may be even more strongly bonded. Some future work thus lies ahead.

Acknowledgment. This research is supported by an ISF (Israel Science Foundation) grant (53/09) to S.S. Mark Danovich is acknowledged for help with the least-squares fitting described in the paper.

Supporting Information Available: Tables of Cartesian coordinates, figures with optimized structures, point groups and state assignments of all calculated clusters are available for B3P86/St-RECP and B3LYP/aug-cc-pVTZ-PP levels. Plots of the D_e/n vs cluster size (n) for all coinage metal clusters calculated using UB3P86/St-RECP method and eq 1 are also available. This material is available free of charge via the Internet at http://pubs.acs.org.

References

(1) McAdon, M. H.; Goddard, W. A., III. *J. Phys. Chem.* **1988**, *92*, 1352.

(2) Glukhovtsev, M. N.; Schleyer, P. v. R. *Isr. J. Chem* **1993**, *33*, 455.

(3) Danovich, D.; Wu, W.; Shaik, S. *J. Am. Chem. Soc.* **1999**, *121*, 3165–3174.

(4) de Visser, S. P.; Alpert, Y.; Danovich, D.; Shaik, S. *J. Phys. Chem. A* **2000**, *104*, 11223.

(5) de Visser, S. P.; Danovich, D.; Wu, W.; Shaik, S. *J. Phys. Chem. A* **2002**, *106*, 4961.

(6) de Visser, S. P.; Danovich, D.; Shaik, S. *Phys. Chem. Chem. Phys.* **2003**, *5*, 158.

(7) Higgins, J.; Hollebeck, T.; Reho, J.; Ho, T.-S.; Lehmann, K. K.; Rabitz, H.; Scoles., G.; Gutowski, M. *J. Chem. Phys.* **2000**, *112*, 5751.

(8) Brühl, F. R.; Miron, R. A.; Ernst, W. E. *J. Chem. Phys.* **2001**, *115*, 10275.

(9) Fioretti, A.; Comparat, D.; Crubellier, A.; Dulieu, O.; Masnou-Seeuws, F.; Pillet, P. *Phys. Rev. Lett.* **1998**, *80*, 4402.

(10) For a few of the earlier calculations of these bound dimmers, see: (a) Kutzelnigg, W.; Staemler, V.; Gélus, M. *Chem. Phys. Lett.* **1972**, *13*, 496. (b) Olson, M. L.; Konowalow, D. D. *Chem. Phys.* **1977**, *21*, 393. (c) Konowalow, D. D.; Olson, M. L. *Chem. Phys.* **1984**, *84*, 462.

(11) It should be noted that the mixing of these structures is not equivalent to a simple $2s-2p_z$ hybridization effect, as evidenced by the fact that Hartree−Fock (HF) wave function for $^3Li_2$ ($^3\Sigma_u^+$), is unbound and repulsive throughout the internuclear distance of 3Å, despite the significant hybridization of the 2s and $2p_z$ orbitals, more so than in the post HF wave functions.

(12) Higgins, J.; Callegari, C.; Reho, J.; Stienkemeier, F.; Ernst, W. E.; Lehmann, K. K.; Gutowski, M.; Scoles, G. *Science* **1996**, *273*, 629.

(13) Higgins, J.; Ernst, W. E.; Callegari, C.; Reho, J.; Lehmann, K. K.; Scoles, G. *Phys. Rev. Lett.* **1996**, *77*, 4532.

(14) Higgins, J.; Callegari, C.; Reho, J.; Stienkemeier, F.; Ernst, W. E.; Gutowski, M.; Scoles, G. *J. Phys. Chem. A* **1998**, *102*, 4952.

(15) Reho, J.; Higgins, J.; Nooijen, M.; Lehmann, K. K.; Scoles, G.; Gutowski, M. *J. Chem. Phys.* **2001**, *115*, 10265.

(16) (a) Cvitas, M. T.; Soldan, P.; Houston, J. M. *Phys. Rev. Lett.* **2005**, *94*, 033201. (b) Quemener, G.; Honvault, P.; Launay, J.-M.; Soldan, P.; Potter, D. E.; Houston, J. M. *Phys. Rev. A: At., Mol., Opt. Phys.* **2005**, *71*, 032722.

(17) (a) Bondybey, V. E. *J. Chem. Phys.* **1982**, *77*, 3771. (b) Huber, K. P.; Herzberg, G. *Constants of Diatomic Molecules,*; Van Nostrand Reinhold: New York, 1979. (c) Rohlfing, E. A.; Valentini, J. J. *J. Chem. Phys.* **1986**, *84*, 6560.

(18) (a) Cvitas, M. T.; Soldan, P.; Houston, J. M.; Honvault, P.; Launay, J.-M. *Phys. Rev. Lett.* **2005**, *94*, 033201. (b) Cvitas, M. T.; Soldan, P.; Houston, J. M.; Honvault, P.; Launay, J.-M. *Phys. Rev. Lett.* **2005**, *94*, 200402.

(19) McAdon, M. H.; Goddard, W. A., III. *J. Chem. Phys.* **1988**, *88*, 277.

(20) Morse, M. D. *Chem. Rev.* **1986**, *86*, 1049.

(21) Lombardi, J. R.; David, B. *Chem. Rev.* **2002**, *102*, 2431.

(22) de Visser, S. P.; Kumar, D.; Danovich, M.; Nevo, N.; Danovich, D.; Sharma, P. K.; Wu, W.; Shaik, S. *J. Phys. Chem. A* **2006**, *110*, 8510.

(23) See for example, (a) Pyykkö, P. *Angew. Chem., Int. Ed.* **2002**, *41*, 3573. (b) Pyykkö, P. *Chem. Rev.* **1997**, *97*, 597.

(24) See for example: (a) Schwerdtfeger, P. *Angew. Chem., Int. Ed.* **2003**, *42*, 1892. (b) Hakkinen, H. *Chem. Soc. Rev.* **2008**, *37*, 1847. (c) Bao, K.; Goedecker, S.; Koga, K.; Lancon, F.; Neelov, A. *Phys. Rev. B: Condens. Matter Mater. Phys.* **2009**, *79*, 041405(R)

(25) (a) Carmeli, I.; Leitus, G.; Naaman, R.; Reich, S.; Vager, Z. *J. Chem. Phys.* **2003**, *118*, 10372. (b) L'vov, V. S.; Naaman, R.; Tiberkevich, V.; Vager, Z. *J. Chem. Phys. Lett.* **2003**, *381*, 650. (c) Naaman, R.; Vager, Z. *Phys. Chem. Chem. Phys.* **2006**, *8*, 2217.

(26) Frisch, M. J.; Trucks, G. W.; Schlegel, H. B.; Scuseria, G. E.; Robb, M. A.; Cheeseman, J. R.; Montgomery, Jr., J. A.; Vreven, T.; Kudin, K. N.; Burant, J. C.; Millam, J. M.; Iyengar, S. S.; Tomasi, J.; Barone, V.; Mennucci, B.; Cossi, M.; Scalmani, G.; Rega, N.; Petersson, G. A.; Nakatsuji, H.; Hada, M.; Ehara, M.; Toyota, K.; Fukuda, R.; Hasegawa, J.; Ishida, M.; Nakajima, T.; Honda, Y.; Kitao, O.; Nakai, H.; Klene, M.; Li, X.; Knox, J. E.; Hratchian, H. P.; Cross, J. B.; Bakken, V.; Adamo, C.; Jaramillo, J.; Gomperts, R.; Stratmann, R. E.; Yazyev, O.; Austin, A. J.; Cammi, R.; Pomelli, C.; Ochterski, J. W.; Ayala, P. Y.; Morokuma, K.; Voth, G. A.; Salvador, P.; Dannenberg, J. J.; Zakrzewski, V. G.; Dapprich, S.; Daniels, A. D.; Strain, M. C.; Farkas, O.; Malick, D. K.; Rabuck, A. D.; Raghavachari, K.; Foresman, J. B.; Ortiz, J. V.; Cui, Q.; Baboul, A. G.; Clifford, S.; Cioslowski, J.; Stefanov, B. B.; Liu, G.; Liashenko, A.; Piskorz, P.; Komaromi, I.; Martin, R. L.; Fox, D. J.; Keith, T.; Al-Laham, M. A.; Peng, C. Y.; Nanayakkara, A.; Challacombe, M.; Gill, P. M. W.; Johnson, B.; Chen, W.; Wong, M. W.; Gonzalez, C.; Pople, J. A. *Gaussian 03*, revision C.02; Gaussian, Inc.: Wallingford, CT, 2004.

(27) Werner, H.-J.; Knowles, P. J.; Lindh, R.; Manby, F. R.; Schutz, M.; Celani, P.; Korona, T.; Rauhut, G.; Amos, R. D.;

Bernhardsson, A.; Berning, A.; Cooper, D. L.; Deegan, M. J. O.; Dobbyn, A. J.; Eckert, F.; Hampel, C.; Hetzer, G.; Lloyd, A. W.; McNicholas, S. J.; Meyer, W.; Mura, M. E.; Nicklass, A.; Palmieri, P.; Pitzer, R.; Schumann, U.; Stoll, H.; Stone, A. J.; Tarroni, R.; Thorsteinsson, T. *MOLPRO*, version 2006 1; University College Cardiff Consultants Limited: Wales, U.K., 2006; see http://www.molpro.net.

(28) (a) Song, L.; Mo, Y.; Zhang, Q.; Wu, W. *XMVB: An ab initio Non-orthogonal Valence Bond Program*; Xiamen University: Xiamen, China, 2003. (b) Song, L.; Mo, Y.; Zhang, Q.; Wu, W. *J. Comput. Chem.* **2005**, *26*, 514.

(29) Danovich, D.; Filatov, M. *J. Phys. Chem. A* **2008**, *112*, 12995.

(30) Reiher, M. *Theor. Chem. Acc.* **2006**, *116*, 241.

(31) Dyall, K. G. *J. Chem. Phys.* **1997**, *106*, 9618.

(32) Balabanov, N. B.; Peterson, K. A. *J. Chem. Phys.* **2005**, *123*, 064107.

(33) Peterson, K. A.; Puzzarini, C. *Theor. Chem. Acc.* **2005**, *114*, 283.

(34) Dolg, M.; Stoll, H.; Preuss, H.; Pitzer, R. M. *J. Phys. Chem.* **1993**, *97*, 5852.

(35) Pou-Amerigo, R.; Merchan, M.; Nebot-Gil, I.; Widmark, P. O.; Roos, B. *Theor. Chim. Acta* **1995**, *92*, 149.

(36) (a) For Zora calculations of Cu_2, Ag_2 and Au_2, see: van Wüllen, C. *J. Phys. Chem.* **1998**, *109*, 392. (b) For Douglas-Kroll calculations of Au_2 using MP4 and CCSD(T) levels: Hess, B. A.; Kaldor, U. *J. Chem. Phys.* **2000**, *112*, 1809.

(37) Bylaska, E. J.; de Jong, W. A.; Govind, N.; Kowalski, K.; Straatsma, T. P.; Valiev, M.; Wang, D.; Apra, E.; Windus, T. L.; Hammond, J.; Nichols, P.; Hirata, S.; Hackler, M. T.; Zhao, Y.; Fan, P.-D.; Harrison, R. J.; Dupuis, M.; Smith, D. M. A.; Nieplocha, J.; Tipparaju, V.; Krishnan, M.; Wu, Q.; Van Voorhis, T.; Auer, A. A.; Nooijen, M.; Brown, E.; Cisneros, G.; Fann, G. I.; Fruchtl, H.; Garza, J.; Hirao, K.; Kendall, R.; Nichols, J. A.; Tsemekhman, K.; Wolinski, K.; Anchell, J.; Bernholdt, D.; Borowski, P.; Clark, T.; Clerc, D.; Dachsel, H.; Deegan, M.; Dyall, K.; Elwood, D.; Glendening, E.; Gutowski, M.; Hess, A.; Jaffe, J.; Johnson, B.; Ju, J.; Kobayashi, R.; Kutteh, R.; Lin, Z.; Littlefield, R.; Long, X.; Meng, B.; Nakajima, T.; Niu, S.; Pollack, L.; Rosing, M.; Sandrone, G.; Stave, M.; Taylor, H.; Thomas, G.; van Lenthe, J.; Wong, A.; Zhang, Z. *NWChem, A Computational Chemistry Package for Parallel Computers*, version 5.1; Pacific Northwest National Laboratory: Richland, Washington, 2007.

(38) For other computational studies, see: (a) DFT, MP2 and CCSD(T) calculations of the ground states of Au_6 and Au_8clusters: Olson, R. M.; Varganov, S.; Gordon, M. S.; Metiu, H.; Chretien, S.; Piecuch, P.; Kowalski, K.; Kucharski, S. A.; Musial, M. *J. Am. Chem. Soc.* **2005**, *127*, 1049. (b) Structural and electronic properties of silver clusters up to Ag_{21}: Zhao, J.; Luo, Y.; Wang, G. *Eur. Phys. J. D* **2001**, *14*, 309. (c) B3LYP and PW91PW91/LANL2DZ calculations of Cu_n, Ag_n, Au_n ($n = 2-6$): Zhao, S.; Ren, Y.; Wang, J.; Yin, W. *J. Phys. Chem. A* **2009**, *113*, 1075. (d) DFT calculations of silver clusters up to $n=12$, using scalar relativistic model potential: Fournier, R. *J. Chem. Phys.* **2001**, *115*, 2165. (e) PW91 calculations of properties of silver clusters: Pereiro, M.; Baldomir, D. *Phys. Rev. A: At., Mol., Opt. Phys.* **2007**, *75*, 033202. (f) MP2 calculations of gold clusters up to $n=6$ in the ground state sho planar geometries: Bravo-Perez, G.; Garzon, I. L.; Novaro, O. *J. Mol. Struct (Theochem)* **1999**, *493*, 225. (g) DFT with plane wave basis sets of Au clusters find that the transition to 3D starts at An_{15}: Xiao, L.; Wang, L. *Chem. Phys. Lett.* **2004**, *392*, 425.

(39) Pereiro, M.; Baldomir, D.; Arias, J. E. *Phys. Rev. A: At., Mol., Opt. Phys.* **2007**, *75*, 063204.

(40) Full configuration-interaction study of the tetrahedral Li_4 cluster confirmed the nature of the no-pair bond by an independent method: Monari, A.; Pitarch-Ruiz, J.; Bendazzoli, G. L.; Evangelisti, S.; Sanches-Martin, J. *J. Chem. Theory and Computations* **2008**, *4*, 404.

(41) Glendening, E. D.; Badenhoop, J. K.; Reed, A. E.; Carpenter, J. E.; Bohmann, C. M.; Morales, C. M.; Weinhold, F. *NBO 5.0*, Theoretical Chemistry Institute: University of Wisconsin, Madison, WI, 2001.

(42) Pyykkö, P.; Desclaux, J.-P. *Acc. Chem. Res.* **1979**, *12*, 276.

(43) Shaik, S.; Hiberty, P. C. *A Chemist's Guide to Valence Bond Theory*, Wiley-Interscience: New York, 2007.

CT100088U